A dissipative particle dynamics method for modeling the geometrical packing of filler particles in polymer composites

J. A. Elliott[a] and A. H. Windle
Department of Materials Science & Metallurgy, University of Cambridge, Pembroke Street, Cambridge, CB2 3QZ, United Kingdom

(Received 1 May 2000; accepted 14 September 2000)

A method is presented for modeling the geometrical packing of polydisperse mixtures of both spherical and nonspherical particles, which are models for filler particles used in the manufacture of polymer composites. The technique is based on the calculation of the dissipative dynamics of an ensemble of fused soft spheres at constant temperature and pressure. After validation of the method at low pressures by comparison with analytical equations of state for monodisperse and binary mixtures of hard spheres, the random packing of fused soft sphere cubes was studied. The effect of packing cubes together with spheres of varying size was then examined, with the aim of developing an understanding of how to minimize the amount of void space in composites containing angular particles. In one case, entropically driven demixing was observed in a cube-sphere mixture.
 [S0021-9606(00)50846-0]

I. INTRODUCTION

Polymer composites are an industrially important class of material in which the mechanical and elastic properties of a polymer matrix are enhanced by loading with filler particles such as glass and carbon fibers, quartz grains, glass beads, and a wide range of other granular media. The geometrical packing of the filler material is crucial in determining the degree of loading which can be achieved,[1–3] together with the rheological properties of the mixture.[4] We have developed a method of studying the geometrical packing of polydisperse blends of spherical and nonspherical particles by calculating the dissipative particle dynamics of rigid assemblies of fused soft spheres.

The geometrical limits to filling space with nontessellating solids has long been of interest, and it is well known that the ratio of particle volume to bulk volume (the packing fraction) for spheres of a single size cannot exceed $\pi/\sqrt{18} \simeq 0.74$. This limit can be exceeded by using spheres of different sizes, and there have a number of experiments involving binary mixtures of colloidal hard spheres which form superlattice crystals[5,6] in which packing fractions higher than 0.74 can be achieved. Simulation work by Eldridge and co-workers[7–9] subsequently elucidated the full phase diagram of such systems, and showed that entropic effects alone are sufficient to stabilize the formation of surprisingly complex structures. More recently, a Monte Carlo study by Zhang and co-workers[10] attempted to find the optimal quasi-continuous size distribution for a fixed number of hard spheres with fixed total volume. They found a tendency for the size distribution to become bimodal above a packing fraction of 0.26.

However, such ordered structures typically evolve over long time scales and in practice the mixtures are often trapped in a glassy state, especially for spheres with certain size ratios.[9] Theoretical studies of binary mixtures of soft spheres, with repulsive pair interactions of the form $\phi(r) = \epsilon(\sigma/r)^n$, have also indicated that an appropriate choice of interaction parameters can strongly inhibit crystallization,[11,12] although softer spheres appear to crystallize more readily than harder ones.[13] The main barrier to observing crystallization in simulations is the strong dependence of nucleation rate on system size and the degree of supercooling,[14,15] which makes it difficult to study the dynamics of crystallization. Although the barrier from fluid to crystal was shown to be crossed by a purely diffusive process for soft spheres,[14,15] it has been suggested that hydrodynamic effects may be important in achieving equilibrium in ordered mesophases of more complex systems.[16–18] We have therefore chosen to use a dissipative particle dynamics method, which preserves hydrodynamics, to study the packing of mixtures of nonspheroidal particles of varying size. Work is currently in progress to include shear in the simulations, in order to study dilatancy phenomena, where hydrodynamics will also be important.

Dissipative particle dynamics (DPD), a technique introduced by Hoogerbrugge and Koelman,[19,20] is very similar to molecular dynamics (MD) but applied on a supramolecular size scale. The dynamics of a system of interacting particles is coarse grained by calculating the motion of particle clusters subjected to pairwise dissipative and random (''Brownian'') forces. These two forces combine to create a continuous pseudofluid in which the particles are suspended and free to interact hydrodynamically. In addition to the hydrodynamic interaction, the particles are prevented from overlapping by an inverse power law soft repulsive force which is conservative in nature.

It is important that all the forces in the system are pairwise acting, so that Newton's third law is strictly obeyed. This, together with Galilean invariance, is sufficient to generate realistic hydrodynamic behavior on time and length

[a]Electronic mail: jae1001@cam.ac.uk

scales not much greater than the time step and the average interparticle separation, respectively.[21] In fact, the Navier–Stokes equations for the mass and momentum density fields have been rigorously derived from DPD by Español[22] using projection operators. In this respect, it is superior to Brownian dynamics,[23] in which the dissipative and random forces are applied with respect to the rest frame of the simulation.

In this paper, we have applied the DPD technique to a system of purely repulsive inverse power law soft spheres which are rigidly fused to form particulates of varying shape and size. The aim was to develop a general method for studying the geometrical packing of irregularly shaped filler particles in composite materials. First, we will describe and validate the method by applying it to monodisperse and binary mixtures of soft spheres, which can be described by existing analytical theories.[24] The effect of angularity on packing is then examined by simulating ''cubes'' formed by rigidly fusing together soft spheres. Finally, we will study a binary mixture of cubes and spheres, in which the diameter of the spheres is varied in an attempt to minimize the void space.

II. METHOD

A. Modeling particulate materials

1. Definitions of ''size'' and ''shape''

There have been a number of published studies concerned with the properties of inverse power law spheres, i.e., those with pair potentials of the form $\phi(r)=\epsilon(\sigma/r)^n$, where n varies from a molecularly soft value of 12[25] to over 200.[26] The size of these soft spheres is usually characterized by forming an equivalence with a hypothetical hard sphere system using perturbation theory. In their paper on liquid-state theory,[27] Barker and Henderson (BH) derived an expression for the equivalent hard sphere diameter of particles interacting under a general pair potential $\phi(r)$ given by Eq. (1), in which $\beta=(k_BT)^{-1}$.

$$d^{\mathrm{BH}}=\int_0^\infty \{1-\exp[-\beta\phi(r)]\}dr. \tag{1}$$

In the case where $\phi(r)=\epsilon(\sigma/r)^n$, the integral (1) can be evaluated explicitly[24] to yield

$$d^{\mathrm{BH}}=\sigma(\beta\epsilon)^{1/n}(1+\gamma/n)+O(1/n^2), \tag{2}$$

where γ is Euler's constant ($\gamma\approx 0.5772$). It is clear from Eq. (2) that the BH diameter tends to σ as n becomes large, i.e., hard spheres with diameter σ are recovered in the limit of infinite ''hardness.'' Since the BH diameter for soft spheres is only dependent on the temperature of the system it is rather unrealistic, especially for dense systems. More sophisticated perturbation theories, such as the Andersen–Weeks–Chandler ''blip-function'' approach,[28] produce superior predictions in this regime.

There have been several relatively successful attempts to construct equivalences for nonspheroidal particles, in particular the hard convex body equation of Boublík and Nezbeda.[29] Recently, more general methods for obtaining simple equations of state for such particles have been published by several different authors.[30,31] However, all these techniques break down in the geometrical packing regime (i.e., where translational symmetry is broken) or when applied to highly angular particles, where relative orientation becomes important.[32] This is because they involve mapping a three-dimensional arbitrarily shaped particle system onto an equivalent spherically symmetric system. Such procedures effectively ''sphericalize'' the particles, and it is therefore not surprising that they do not accurately describe the subtle packing behavior of angular particles.

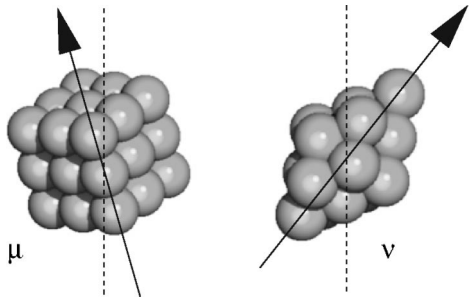

FIG. 1. The force between two angular particles μ and ν of arbitrary shape and relative orientation is calculated by summing the forces between each pair of soft spheres i and j in each particle.

In this paper, the problem of dealing with deviations from spherical symmetry is dealt with by considering each irregular particle to be represented by the center of mass and three principal moments of inertia of a rigid assembly of fused soft spheres. By using this representation, the complicated problem of calculating the force between two adjacent particles, labeled μ and ν, of arbitrary shape and relative orientation is replaced by the trivial task of summing the forces acting between each pair of component spheres, labeled i and j, in the two particles: $\mathbf{F}_{\mu\nu}=\Sigma_{i,j}\,\mathbf{f}_{ij}$. This is illustrated in Fig. 1, and results in a net force and torque on each particle which accurately reflects the true shape of the excluded volume.

The fused sphere representation has been applied previously to model the random packing of fibers by Evans and Ferrar,[33] but they used hard spheres combined with Monte Carlo insertion and settling. The use of hard spheres with the DPD algorithm is complicated by the mixture of continuous and impulsive forces which such a simulation would require. Although methods have been devised to combine hard core repulsions with continuous tails in MD simulations,[34,35] their application here is complicated due to the need to unravel the correlated motions of the rigid bodies. However, excluded volume effects can be achieved using just soft repulsive forces, together with extrapolation of the repulsive exponent to large values. The problem is how to define a length scale for such a system in order to calculate a realistic packing fraction.

The size of such angular particles cannot be calculated as a perturbation to a spherically symmetric system, as the distance of closest approach depends so strongly on relative orientation. Instead, the volume of each particle can be approximated by the sum of the BH volumes of each sphere from which it is comprised. However, there are a number of problems with this approach. The principle objection is that the BH diameter is only strictly valid for a free fluid of soft

spheres, although it is apparent from simulations that the packing fraction of pressurized fluids of fused spheres becomes increasingly insensitive to the value of the repulsive exponent in the limit of large n. It is also necessary to take into account the volume of any interstitial gaps at the surface or in the bulk of a particle. In this study, we approximate the volume of a fused soft sphere particle by that of a polyhedron with vertices at the centers of the apical spheres. This procedure is justified by the fact that adjacent particles of a similar size will not be able to occupy the interstitial volume. However, there is a need for caution when considering mixtures of particles with a broad distribution of sizes.

2. Effects of varying size and shape

In order to derive a realistic value for the packing fraction ξ of a suspension of particulates of various shapes and sizes, the mixture must be simulated under bulk conditions. In this case, ξ is defined as the ratio of total volume occupied by solid particles to the volume of the pseudoperiodic unit cell. The cell volume may be kept fixed or, alternatively, it may be allowed to reach equilibrium at a constant hydrostatic pressure. By varying the magnitude of the pressure relative to the level of thermal noise, structural reorganizations in the packing of the particulate phase may be observed. In the context of real systems, the thermal noise represents mechanical agitation and the pressure is produced by the weight of the particles. There is also a more subtle pressure effect due to the presence of a viscous pore fluid that binds the fillers, e.g., epoxy resin, which acts to resist any increase in bulk volume.

As the size and shape of the particles are varied, the applied pressure should be changed in order to keep the packing fraction of the particles nominally constant. By this, we mean that the physical pressure should be reduced using a simple scaling relation involving the volumes of each type of particle weighted by their relative concentrations. In the case of a binary mixture of hard spheres, with diameters d_1 and d_2 and mole fractions x_1 and x_2, such a relation is given by Eq. (3). This is the van der Waals one-fluid approximation,[24] which is exact at low packing fractions but fails at higher packing fractions where geometrical effects become significant. It is these geometrical effects which we wish to study, especially for systems involving highly angular particles.

$$p^* \equiv \beta p_{\mathrm{eq}}(x_1 d_1^3 + x_2 d_2^3). \tag{3}$$

The rigid cubes studied in Sec. III B were constructed from 26 spheres arranged in a cubic array (the central sphere being omitted). One-hundred twenty-five such units, comprising a total of 3250 spheres, were simulated from an initial configuration consisting of a simple cubic superlattice with a spacing equal to twice the side-length l of each cube. In this case, the side length of a cube is defined as the distance between the centers of spheres at adjacent vertices plus one BH diameter (all spheres having the same diameter). The reduced pressure for a mixture of spheres and cubes is then given by Eq. (4), where x_1 and x_2 are the mole fractions of spheres and cubes, respectively. It should be noted that the packing fraction calculated using l will be subject to small systematic errors due to the possibility of adjacent cubes interpenetrating without appreciable overlap of their constituent spheres.

$$p^* \equiv \beta p_{\mathrm{eq}}(\pi x_1 d^3/6 + x_2 l^3). \tag{4}$$

B. Dissipative particle dynamics algorithm

1. Force interactions

The force interactions between spheres in the rigid bodies can be summarized by

$$\mathbf{F}_{ij}^C = (n\varepsilon_{ij}/\sigma_{ij})\omega^C(\sigma_{ij}/r_{ij})^{n+1}\hat{\mathbf{r}}_{ij}, \tag{5}$$

$$\mathbf{F}_{ij}^D = -\kappa\omega^D(\hat{\mathbf{r}}_{ij}\cdot\mathbf{v}_{ij})\hat{\mathbf{r}}_{ij}, \tag{6}$$

$$\mathbf{F}_{ij}^R = \lambda\omega^R\theta_{ij}\Delta t^{-1/2}\hat{\mathbf{r}}_{ij}, \tag{7}$$

where Eq. (5) is the conservative soft power law repulsive force, Eq. (6) is the dissipative force, and Eq. (7) is the random ''Brownian'' force which act between two spheres i and j whose centers are connected by a vector $\mathbf{r}_{ij}$ and travel with relative velocity $\mathbf{v}_{ij}$. The parameters ε_{ij} and σ_{ij} define the relative ''size'' of the spheres i and j [via Eq. (2)], and θ_{ij} are a set of Gaussian random numbers with zero mean and unit variance. Typical numerical values for these parameters were $n=12$, $\sigma=5$ Å, $\varepsilon=10^{-10}$ kcal mol^{-1}, $\kappa=0.6$ amu ps^{-1}, and $\lambda=1.0$ amu Å ps$^{-3/2}$. It should be noted that the repulsive potential is significantly harder than that used in some previous applications of DPD.[36,37]

Español and Warren[21] showed that if the weight functions ω^D and ω^R are chosen to satisfy a fluctuation–dissipation theorem, then an equilibrium temperature is established in the simulation. The functions used in the present study are very similar to those of Groot and Warren,[36] but include an explicit cutoff distance r_c which was typically set to twice the size of the largest particle in the simulation,

$$\omega^C = \begin{cases} 1, & r < r_c \\ 0, & r \geqslant r_c, \end{cases} \tag{8}$$

$$\omega^D = \begin{cases} (1-r/r_c)^2, & r < r_c \\ 0, & r \geqslant r_c, \end{cases} \tag{9}$$

$$\omega^R = \begin{cases} (1-r/r_c), & r < r_c \\ 0, & r \geqslant r_c. \end{cases} \tag{10}$$

The friction coefficient κ and the noise amplitude λ are connected by Eq. (11), where T_{eq} is the desired equilibrium temperature of the simulation. The appearance of the time step Δt in the expression for the random force, Eq. (7), is due to the effect of time discretization in the integration algorithm, and the origins of this have been discussed in detail by several authors.[36,38] The actual time step used was typically 10^{-3} ps, which is of order 10^{-4} when expressed in dimensionless units of $r_c(\beta m)^{1/2}$.

$$\lambda^2 = 2\kappa k_B T_{\mathrm{eq}}. \tag{11}$$

2. Equations of motion

The equations of motion for our system are given by Eqs. (12)–(15). These are based on the combined thermostat and barostat proposed by Hoover[39] and subsequently refor-

mulated by Melchionna,[40] which is commonly used in standard NpT MD simulations. However, in this system the thermostat has been completely removed, and the barostat has been decoupled from the translational degrees of freedom of the particles. This is necessary in order to ensure that collisions between particles conserve momentum. An equilibrium temperature is then established by the DPD force interactions, given by Eqs. (5)–(7), which act pairwise between each component sphere so that Newton's third law is obeyed,

$$\dot{\mathbf{r}}_i = \mathbf{v}_i + \eta \mathbf{r}_i , \tag{12}$$

$$\dot{\mathbf{p}}_i = \mathbf{F}_i , \tag{13}$$

$$\dot{\eta} = \frac{1}{\tau_p^2} \frac{1}{N k_B T_{\mathrm{eq}}} (p(t) - p_{\mathrm{eq}}), \tag{14}$$

$$\dot{V} = 3V\eta. \tag{15}$$

The time evolution of the particle coordinates $\mathbf{r}_i$ is calculated from Eq. (12), where η is a fictitious dynamical variable that compensates for any difference between the instantaneous pressure, defined by Eq. (16),[23] and the desired equilibrium pressure p_{eq}. The simulation box volume V relaxes to its equilibrium value with a characteristic time τ_p.

$$p(t) \equiv (3V)^{-1} \sum_i \left(\mathbf{p}_i^2 / m_i + \mathbf{F}_i \cdot \mathbf{r}_i \right). \tag{16}$$

In the Appendix, we show that these modified equations of motion sample from a pseudo-Boltzmann constant pressure ensemble which involves the instantaneous temperature of the simulation. Thus, when used in combination with the DPD force interactions described in Sec. II B 1, the simulation as a whole relaxes to an equilibrium temperature T_{eq} and equilibrium pressure p_{eq}. By setting the relative levels of T_{eq} and p_{eq}, the assemblies of particulates can be mixed or packed densely together as desired.

The DPD algorithm was implemented using a modified version of the general purpose parallel MD package DL_POLY (version 2.11), developed by CCP5 of the EPSRC.[41] DL_POLY was chosen principally due to its ability to handle rigid body dynamics using Fincham's implicit quarternion algorithm.[42] The equations of motion were integrated using the standard Verlet leapfrog method.[43,44] Both the thermostration and barostration were found to be very accurate (no detectable drift after 10^6 time steps) and reasonably precise (typical standard deviation of up to 5% from the mean).

III. RESULTS

A. Validation of method

1. Monodisperse soft spheres

The next stage of validation was to check the packing behavior of the simplest type of particle: soft spheres of a single size. For such systems, the density is purely a function of the reduced pressure defined by $p^* \equiv \beta p_{\mathrm{eq}} d^3$, where d is the effective diameter of the spheres. At low reduced pressures, the BH diameter defined by Eq. (1) gives a reasonable estimate of d. The DPD simulations were compared against theoretical results using the Carnahan–Starling equation of state for hard spheres,[45] which is known to be very accurate for the fluid phase.[46,47] The packing fraction, $\xi \equiv (N/V) \times (\pi d^3/6)$ is shown as a function of reduced pressure in Fig. 2. The results from the DPD simulations are in very close agreement at low reduced pressures, but diverge as the pressure is increased. This is mainly because the BH diameter overestimates the effective size of the spheres at high pressures. Nevertheless, the point is that the DPD simulations accurately reproduce the packing behavior of soft spheres in the regime where an equivalence can be made with analytical expressions for hard spheres.

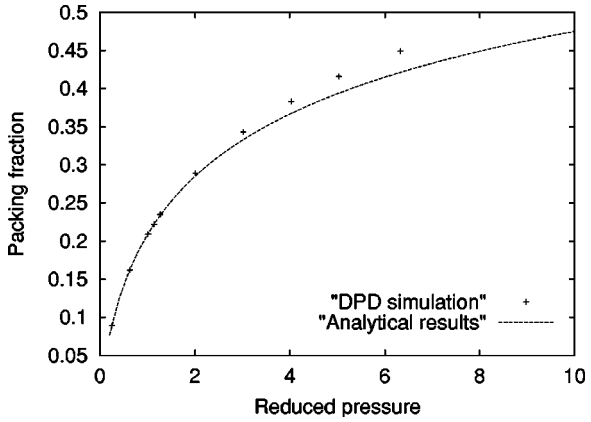

FIG. 2. Packing fraction as a function of reduced pressure for a monodisperse soft sphere system: DPD simulations (points) and Carnahan–Starling equation (line). Statistical errors in the simulation data are represented by the size of each point.

2. Binary mixtures of polydisperse soft spheres

The predictions of the DPD method for mixtures of soft spheres of varying size and relative concentrations were tested against the Boublík–Mansoori (BM) equation of state for hard spheres,[48,49] using BH diameters with a van der Waals one-fluid mixing rule. In this case, we define the reduced pressure using Eq. (3), where x_i and d_i are the mole fractions and BH diameters of the two components, respectively. The packing fraction of the binary mixture $\xi \equiv \xi_1 + \xi_2$, where $\xi_i \equiv x_i (N/V)(\pi d_i^3/6)$, is a function of three parameters: reduced pressure, diameter ratio, and concentration of one component.

Figure 3 is a two-dimensional map of the packing fraction of a binary mixture of soft spheres predicted from the BM equation of state at a reduced pressure $p^* = 1.0$ as a function of diameter ratio d_2/d_1 and mole fraction of the second component x_2. Figure 3 shows that there is a broad minimum in the packing fraction when the components are similar in size and number, with the density increasing rapidly as component 2 becomes smaller and more numerous than component 1. Figure 3 is not symmetrical, as the total volume of the components is changing at fixed reduced pressure. A line section through this surface at $x_2 = 0.5$ is shown in Fig. 4, along with the corresponding DPD results. The agreement is good, and demonstrates that the method provides an accurate model of mixtures of different sized particles in the fluid phase, where comparison can be made with analytical theories for hard spheres.

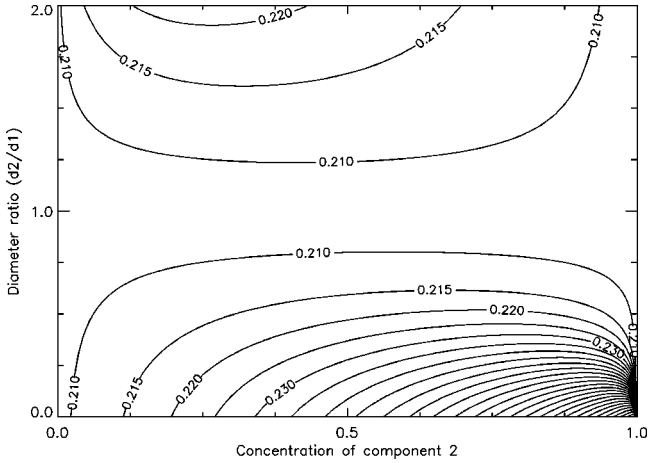

FIG. 3. Packing fraction of a binary soft sphere mixture from the Boublík–Mansoori equation, where d_2/d_1 is the ratio of the Barker–Hendreson diameters and x_2 is the mole fraction of the second component.

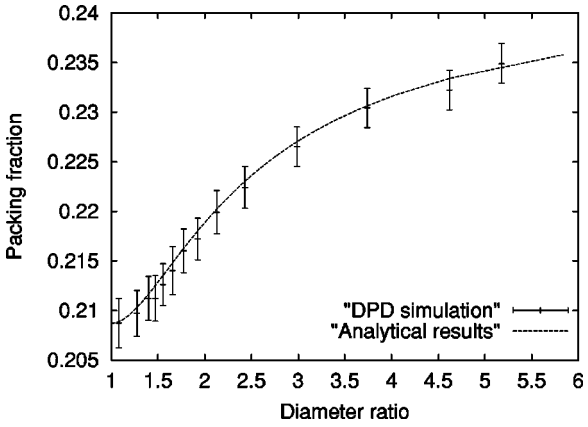

FIG. 5. Packing fraction of a binary soft sphere mixture as a function of diameter ratio $e=d_2/d_1$ at $p^*=1.0$ with a constant volume of the components ($x_1d_1^3+x_2d_2^3$ constant). Comparison between DPD simulations (bars) and Boublí–Mansoori equation (line).

The DPD method was also tested on binary mixtures with a constant volume of components at fixed concentration, i.e., where the diameter ratio is adjusted in such a way as to transfer a fixed amount of volume ΔV from one component to the other. In this case, the surface in Fig. 3 is symmetrical, and a half-section at $x_1=x_2=0.5$ is shown in Fig. 5 along with the corresponding DPD results. Again, the agreement is good for diameter ratios as high as 6:1. At higher reduced pressures, the BH diameter ceases to be a useful measurement of particle size. However, this does not affect the fundamental variation of density as a function of reduced pressure and, in the case where rigid assemblies of fused spheres are used, represents only a small part of the overall particle size.

B. Simulations of cubic particles

Having validated the DPD method by obtaining a good correspondence with analytical results for free spheres, we now consider the packing of fused assemblies of soft spheres. The reduced pressure is defined as $p^*\equiv\beta p l^3$, where l is the side length of the cubes defined in Sec. II A 2, and the packing fraction as $\xi\equiv(N/V)l^3$. The simulations were carried out at high pressures in order to study the effects of relative orientation on packing, and therefore the packing fraction is slightly ambiguous as the edges of the cubes are ''soft.'' However, it should be emphasized that the cubes themselves remained completely rigid during the simulations.

As the reduced pressure was increased, various changes in the orientational and positional ordering of the cubes were observed. Figure 6 shows simulations at $p^*=10.0$ and $p^*=20.0$, where the cubes have been visualized by constructing cubes of side-length l centered on each fused unit of soft spheres. At $p^*=10.0$, Fig. 6(a), the cubes display little orientational ordering and the packing fraction is relatively low ($\xi=0.582$). However, at $p^*=20.0$, as shown in Fig. 6(b), the only way for the cubes to pack more efficiently ($\xi=0.730$) is to form a distorted lattice. Although the registration between cubes is not perfect, their orientations have clearly become much more correlated than in Fig. 6(a).

The radial distribution functions of the cube centers for the simulations at $p^*=10.0$ and $p^*=20.0$ are shown in Fig. 7, along with the radial distribution function (RDF) for an ideal lattice for comparison. This demonstrates clearly that the cubes are far from being crystalline in both cases, al-

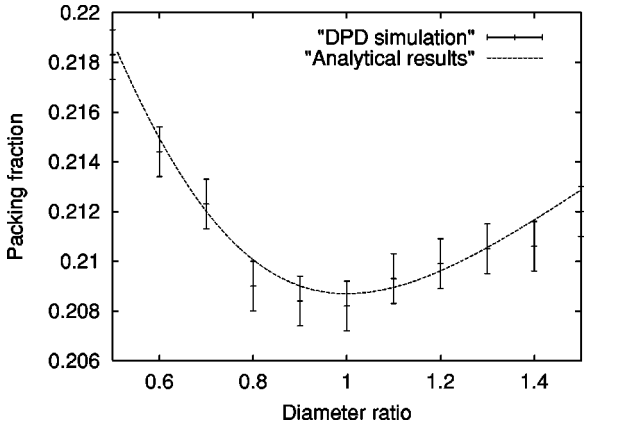

FIG. 4. Packing fraction of a binary soft sphere mixture as a function of diameter ratio $e=d_2/d_1$ at $p^*=1.0$ for equal mole fractions $x_1=x_2=0.5$ of the components. Comparison between DPD simulations (bars) and Boublík–Mansoori equation (line).

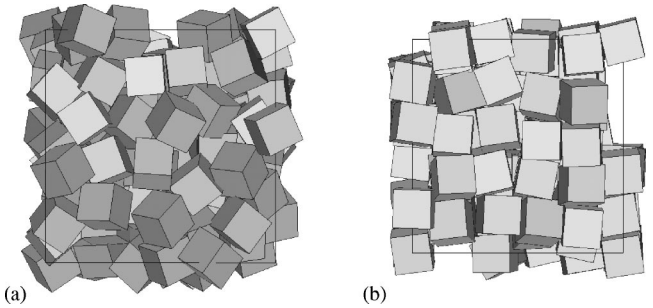

FIG. 6. Visualization of fused soft sphere cubes packed at reduced pressures of (a) $p^*=10.0$ and (b) $p^*=20.0$. The packing fractions were $\xi=0.582$ and 0.730, respectively. The figures are shown to scale.

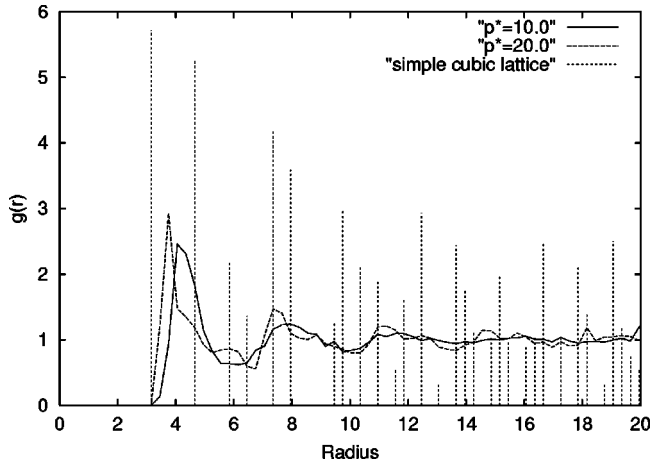

FIG. 7. Radial distribution functions of the fused soft sphere cubes shown in Fig. 6, along with the RDF from an ideal simple cubic lattice for comparison.

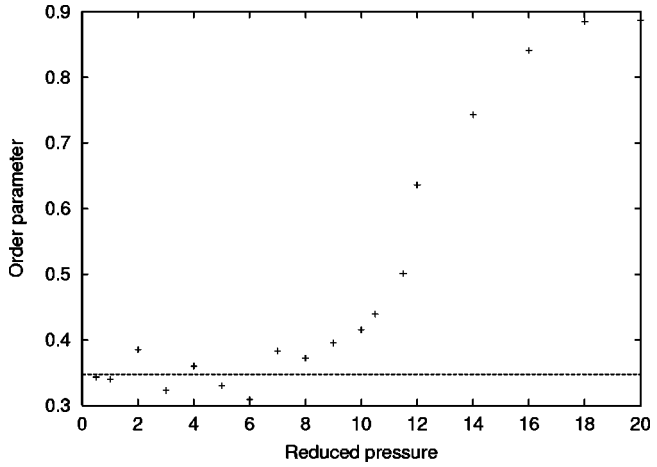

FIG. 9. Orientational order parameter $\langle P_2 \rangle$ of fused soft sphere cubes as a function of reduced pressure. The value of $\langle P_2 \rangle$ for an isotropic array is given by the dotted line.

though there is a noticeable sharpening of the {100} and {210} peaks.

In Fig. 8 the packing fraction of the cubes is plotted as a function of reduced pressure, together with the results for monodisperse spheres from Fig. 2 for comparison. Despite the qualitative change in the orientational and positional ordering of the cubes shown in Fig. 6, there is no discontinuity in this curve to suggest a freezing transition. This is not surprising, as the transition is only some 10% for hard spheres. However, a plot of the first axially symmetric orientational order parameter $\langle P_2 \rangle$ of the cube edges against reduced pressure, shown in Fig. 9, does exhibit a transition. The order parameter was calculated by choosing a director such that $\langle P_2 \rangle$ over all the cube edges is maximized, with the dotted line indicating the value of $\langle P_2 \rangle$ for an isotropically oriented array of cubes. It can be seen that there is an apparently Landau-type isotropic–cubatic transition at around $p^* = 10.0$. The cubatic phase is an orientationally ordered phase with cubic symmetry, observed previously in studies of cut hard spheres by Veerman and Frenkel.[50] We describe the ordered phase, shown in Fig. 6(b), as cubatic rather than cubic due to the lack of long-range translational order.

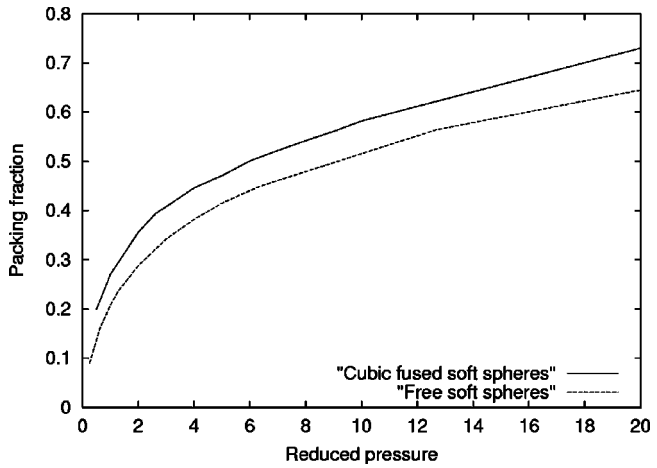

FIG. 8. Packing fraction of fused soft sphere cubes as a function of reduced pressure, compared against the DPD results for free soft spheres (from Fig. 2).

C. Simulations of mixtures of spherical and cubic particles

Given a partially ordered packing of large angular particles, such as those studied in Sec. III B, it is interesting to ask how the interstices may best be filled in order to improve the loading of the composite material. To address this issue for randomly packed cubes, we examined the changes in packing density which can be achieved by mixing spheres of various sizes with fused sphere cubes. The simulations were carried out for mixtures containing equal numbers of cubes and spheres at fixed reduced pressure, defined by Eq. (4), where l and d are the side length of the cubes and diameter of the spheres, respectively. The parameter for the simulations was the ratio d/l, with the physical pressure being adjusted in each case to maintain a constant reduced pressure of $p^* = 20.0$. Reducing the pressure in this way has the effect of isolating changes in the packing fraction due to purely geometrical effects.

Simulations at four values of d/l are visualized in Fig. 10. With no spheres present, i.e., at $d/l = 0$, the cubes were able to pack with a high degree of order, shown in Fig. 10(a). When spheres with $d/l = 0.549$ were added, shown in Fig. 10(b), the degree of order was reduced by the need to accommodate them into the structure. This resulted in a drop in packing fraction from 0.730 to 0.716, with an appreciable disruption of the correlation between the orientations of adjacent cubes. When $d/l = 1.020$, shown in Fig. 10(c), the spheres were too large to effectively fill the interstices made by the cubes, resulting in widespread disruption of the cubic superlattice, with the packing fraction dropping to 0.680. At $d/l = 1.804$, shown in Fig. 10(d), the packing fraction rose again to 0.705. This is due to the cubes beginning to fill the interstices made by the spheres, as the latter become larger than the former.

The full dependence of the packing fraction of the cube–sphere mixtures on d/l is shown in Fig. 11. The dotted line

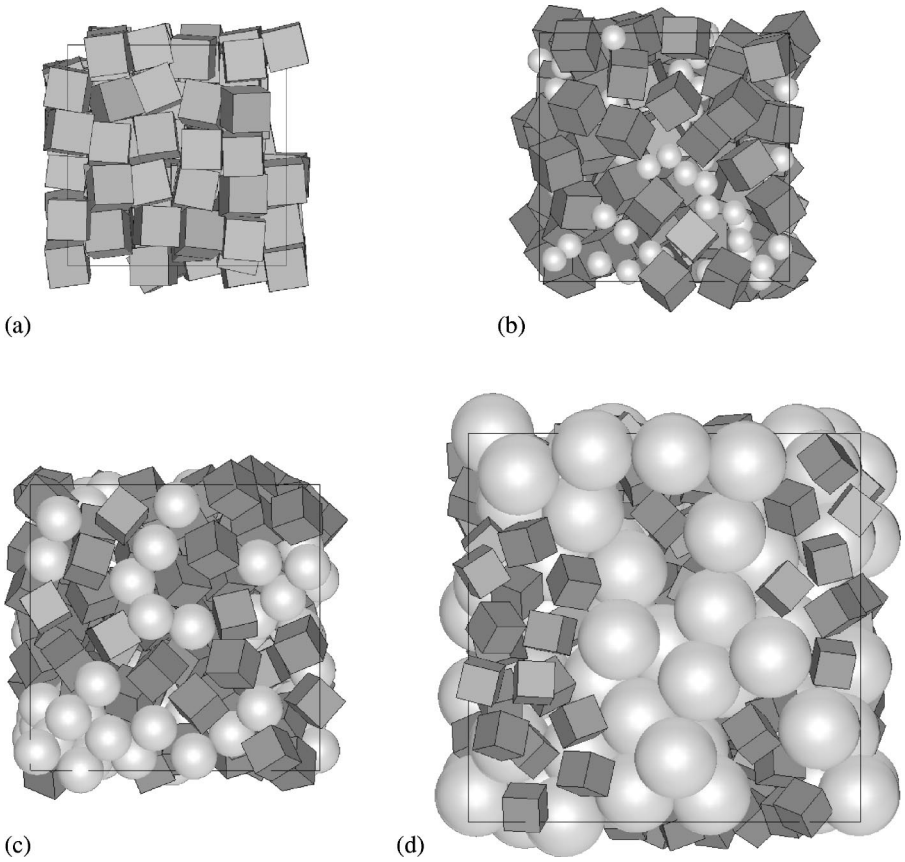

FIG. 10. Visualization of a mixture of fused soft spheres (side-length l) with free soft spheres (diameter d) at fixed reduced pressure $p^*=20.0$ as a function of d/l: (a) no spheres, (b) $d/l=0.549$, (c) $d/l=1.020$, and (d) $d/l=1.804$. The packing fractions were $\xi=0.730$, 0.716, 0.680, and 0.705, respectively. The figures are shown to scale.

shows the packing fraction achieved by pure cubes at $p^*=20.0$, and the dashed line that achieved by pure spheres at this pressure. It should be pointed out that the physical pressure changes nonlinearly from left to right in Fig. 11 in order to maintain a constant reduced pressure. The graph shows that the packing fraction of the mixtures is largest for small values of d/l and falls at a constant rate until reaching a minimum around $d/l=1.2$, where the interstice-filling effect of the spheres is outweighed by the disruption they cause to the packing of the cubes. We would expect to find a maximum in the curve as d/l becomes small, although the point at which this occurs is difficult to determine due to the tendency for smaller spheres to interpenetrate the fused sphere cubes.

Figure 12 shows the dependence of the order parameter $\langle P_2\rangle$ on d/l. The effect of adding spheres is to reduce the orientational order of the cubes, which become effectively isotropic (the level of the dotted line) at around $d/l=1.6$ and above. This behavior is consistent with the drop in packing fraction with increasing d/l seen in Fig. 11, with the onset of isotropic order corresponding to the point where the cubes

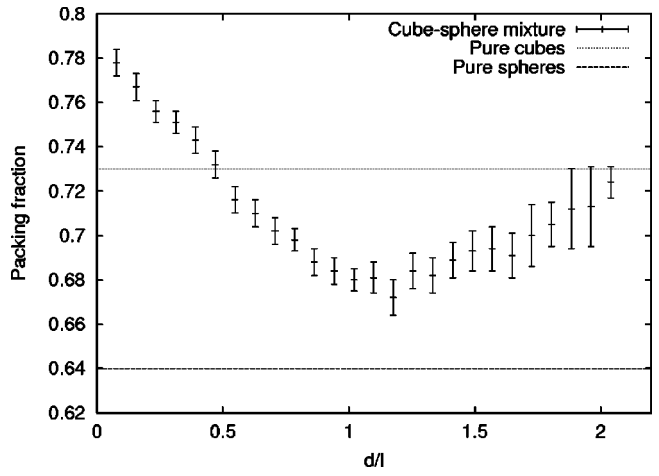

FIG. 11. Packing fraction of a mixture of fused soft sphere cubes and free spheres as a function of the ratio of the diameter of the spheres to the side length of the cubes at $p^*=20.0$.

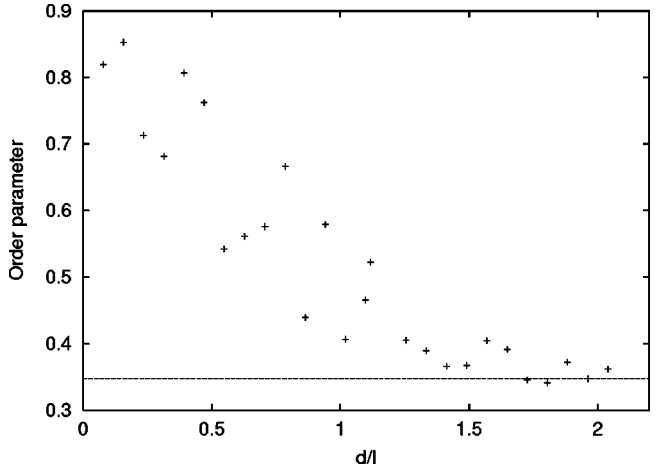

FIG. 12. Orientational order parameter $\langle P_2\rangle$ of a mixture of fused soft sphere cubes and free spheres as a function of the ratio of the diameter of the spheres to the side length of the cubes at $p^*=20.0$. The value of $\langle P_2\rangle$ for an isotropic array is given by the dotted line.

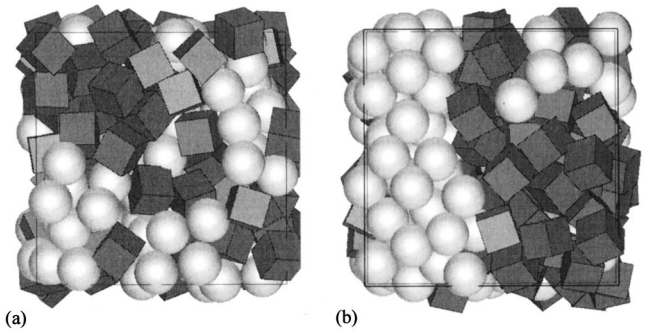

FIG. 13. Visualization of demixing in a mixture of fused soft sphere cubes and free soft spheres with a side-length to diameter ratio of $d/l=1.255$. In (a) the two components are well mixed with $\xi=0.614$, but later in the simulation (b) the components separated, with a drop in packing fraction to $\xi=0.580$. In (b), the periodic boundary of the mixed simulation (given by the thinner line) is shown for comparison with that of the demixed simulation (thicker line).

are incorporated within interstices formed by the spheres. The disordering may also be explained by the smaller physical pressures at higher values of d/l, which could cause the cubes to undergo a cubatic–isotropic transition as observed in pure cubes in Sec. III B.

A complicating issue is that of demixing between the spheres and cubes. Figure 13 shows a cube–sphere mixture with $d/l=1.255$ which underwent a demixing transition during a simulation. The radial distribution functions of each of the components for the mixed and demixed states, shown in Fig. 14, reflect the demixing by the relative levels of the particle–particle contact peaks. In the demixed state the sphere–sphere and cube–cube contact peaks are greater in magnitude, indicating that a greater proportion of the contacts are between particles of similar shape than in the mixed state.

Such demixing transitions have been observed in purely entropic systems, including binary mixtures of hard cubes on a lattice[51] and hard ellipsoidal rod-plate mixtures,[52] and are the subject of a recent review by Frenkel.[53] The simulations described here have an additional enthalpic factor associated with changes in the total volume of the system. This will tend to favor arrangements which minimize the total volume. However, as shown in Fig. 13, the packing fraction falls on demixing, from $\xi=0.614$ to 0.580, which implies that there is an enthalpic barrier to demixing. In order for this to occur spontaneously, the particles must have gained entropy. This is most probably in the form of translational entropy due to the increased amount of free volume per particle.

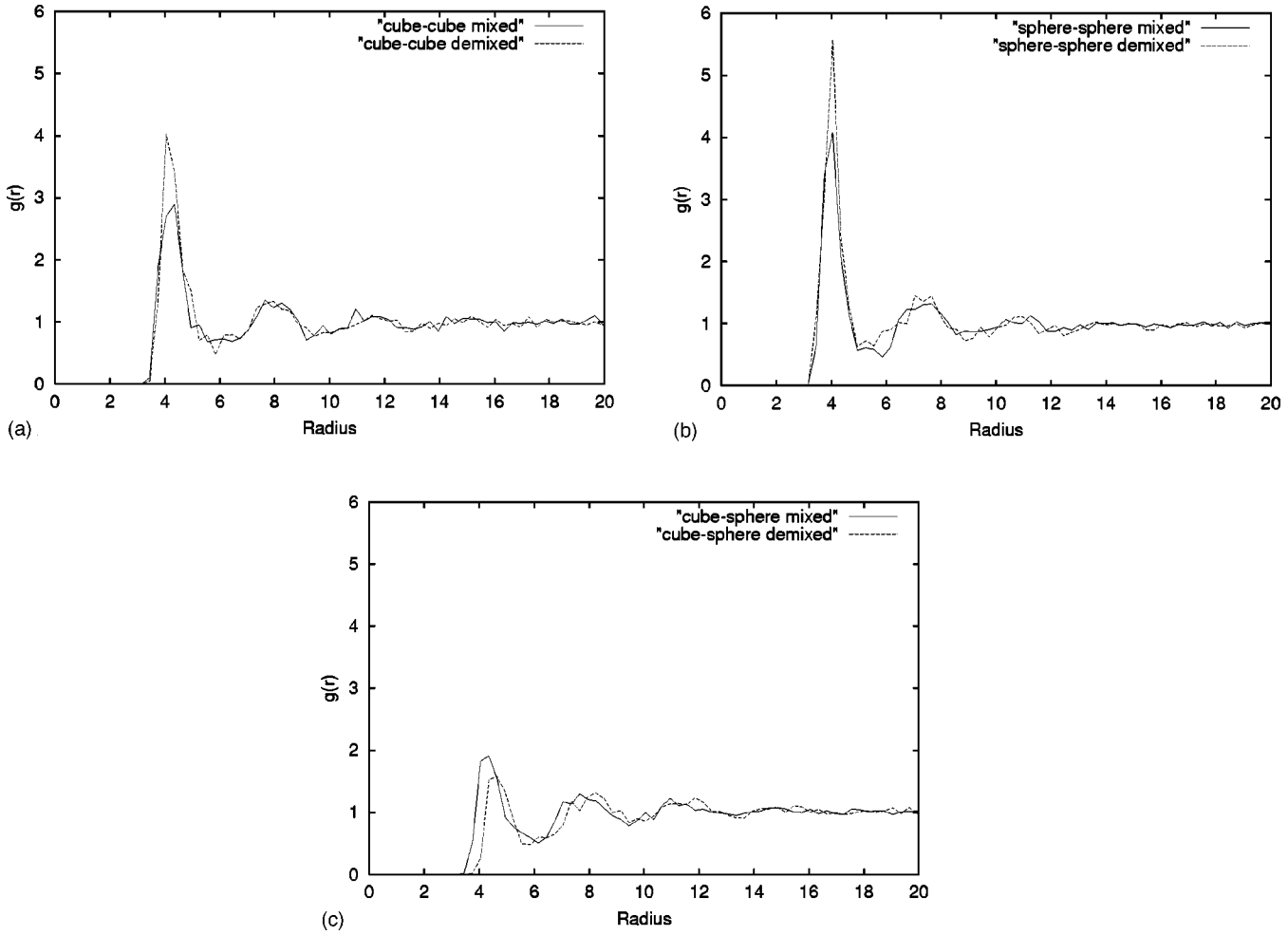

FIG. 14. Radial distribution functions of the mixed and demixed simulations of fused soft sphere cubes and free soft spheres with a diameter to side-length ratio of $d/l=1.255$: (a) cube–cube RDFs, (b) sphere–sphere RDFs, and (c) cube–sphere RDFs.

IV. DISCUSSION

We have shown that it is possible to simulate the geometric packing of particles of various shapes and sizes by considering the dissipative particle dynamics of assemblies of free and fused soft spheres at constant pressure. The results for free soft spheres correspond well with analytical results from the Carnahan–Starling and Boublík–Mansoori equations of state in the low pressure regime where an equivalent hard sphere diameter can be used. In the case of a binary mixture of spheres, there was a minimum in the packing fraction when the components were equal in size. We interpret this as being due to the smaller component filling the interstices of the larger component.

In the case of cubic particles, being the simplest example of a nonspheroidal particle, the packing behavior as a function of reduced pressure is similar to that of the spheres. However, there appears to be an isotropic–cubatic transition in the orientational correlation between adjacent cubes. When spheres of various sizes were added to the cubes, the packing fraction increased relative to the pure cube system when $d/l<0.5$, and otherwise decreased, reaching a minimum at $d/l\approx 1.2$. We interpret this behavior as being due to the balance between the interstice-filling effect of the spheres and the disruption of the regular cube packing. The minimum occurs around the expected value of $d/l=(6/\pi)^{1/3}\approx 1.24$, where the individual cubes and spheres are of equal volume.

With regard to demixing, we showed one example of how the increase in translational entropy of the filler particles on demixing is sufficient to overcome the enthalpic barrier due to expansion against an external pressure or pore fluid. It is an open question as to whether the difference in sphericity of the particles raises the barrier to demixing by requiring a larger resultant increase in total volume, or lowers it by providing a higher entropic driving force. However, if it were possible to design a mixture in which demixing produced a large increase in total volume with only a small increase in free volume per particle then we would expect that this mixture would remain well mixed under all conditions.

In the future, we envisage applying the DPD method to a wide range of particle shapes: rigid fibers, mixtures of spheres and spheroids, and mixtures of spheroids and fibers. It will also be possible to carry out nonequilibrium simulations, such as the application of shear forces to packed assemblies, and use of gravitational fields to examine density segregation effects. Attractive forces between particles can easily be incorporated and, with some modifications to the algorithm, it should be possible to simulate flexible particles.

ACKNOWLEDGMENTS

The authors are grateful to the Engineering and Physics Sciences Research Council (EPSRC) for their funding. They also wish to acknowledge the University of Cambridge High Performance Computing Facility for the use of their SGI Origin 2000 computer and associated staff support during the course of this project. The visualizations in Figs. 6, 10, and 13 were performed using the GEOMVIEW package.[54] J.E. wishes to thank Dr D. C. Hoyle for many helpful discussions.

APPENDIX: PROOF THAT EQUATIONS OF MOTION GENERATE A PSEUDO-BOLTZMANN CONSTANT PRESSURE ENSEMBLE

In order to prove that the equations of motion presented in Sec. II B 2 sample a pseudo-Boltzmann constant pressure ensemble with a well-defined instantaneous temperature, we will show that the equilibrium distribution function $f(\mathbf{r}_i,\mathbf{p}_i,V,\eta)$ is proportional to $\exp\{-(3N/2)(H/K)\}$, where H is the enthalpy defined by

$$H=K+U+p_{\mathrm{eq}}V+(3N/2)k_BT_{\mathrm{eq}}\tau_p^2\eta^2. \tag{A1}$$

Following a method of derivation introduced by Hoover[39] and Nosé,[55] we will use the general probability flow equation:

$$\frac{df}{dt}=-f\sum_k\frac{\partial\dot{x}_k}{\partial x_k}, \tag{A2}$$

where $\{x_k\}$ are the dynamical variables.

Substituting the equations of motion (12)–(15) into Eq. (A2), we obtain

$$\begin{aligned}\frac{df}{dt}&=-f\left\{\sum_i\left[\frac{\partial\dot{\mathbf{r}}_i}{\partial\mathbf{r}_i}+\frac{\partial\dot{\mathbf{p}}_i}{\partial\mathbf{p}_i}\right]+\frac{\partial\dot{V}}{\partial V}+\frac{\partial\dot{\eta}}{\partial\eta}\right\}\\&=-f\left\{\sum_i\left[\frac{\partial}{\partial\mathbf{r}_i}\eta\mathbf{r}_i\right]+3\eta\right\}=-3Nf\eta.\end{aligned} \tag{A3}$$

However, since $\Sigma_i\mathbf{F}_i=0$,

$$\begin{aligned}\frac{dH}{dt}&=\sum_i\left(\frac{\partial H}{\partial\mathbf{r}_i}\dot{\mathbf{r}}_i+\frac{\partial H}{\partial\mathbf{p}_i}\dot{\mathbf{p}}_i\right)+\frac{\partial H}{\partial V}\dot{V}+\frac{\partial H}{\partial\eta}\dot{\eta}\\&=-\sum_i\mathbf{F}_i\cdot\left[\frac{\mathbf{p}_i}{m_i}+\eta\mathbf{r}_i\right]+\sum_i\frac{\mathbf{p}_i}{m_i}\cdot\mathbf{F}_i\\&\quad+3V\eta p_{\mathrm{eq}}+3(p(t)-p_{\mathrm{eq}})V\eta\\&=-\eta\sum_i\mathbf{F}_i\cdot\mathbf{r}_i+3V\eta p(t)=\eta\sum_i\frac{\mathbf{p}_i^2}{m_i}=2\eta K.\end{aligned} \tag{A4}$$

Thus, eliminating η between Eqs. (A3) and (A4), we obtain

$$\frac{df}{dt}=-\frac{3Nf}{2K}\frac{dH}{dt},$$

from which follows

$$f\propto\exp\left\{-\frac{3N}{2}\frac{H}{K}\right\},$$

which was the result to be proved. Under the influence of the dissipative and random forces described in Sec. II B 1, the $3N/(2K)$ factor will tend to $(k_BT_{\mathrm{eq}})^{-1}$ by equipartition, subject to fluctuations with magnitude of order $N^{-1/2}$. Thus, an equilibrium distribution will be established at temperature T_{eq} and pressure p_{eq}.

[1] J. Ritter, J. Appl. Polym. Sci. Appl. Polym. Symp. **15**, 239 (1971).
[2] J. V. Milewski, Composites **78**, 258 (1973).
[3] J. V. Milewski, Ind. Eng. Chem. Prod. Res. Dev. **17**, 363 (1978).
[4] E. G. Flekkøy and K. J. Måløy, Phys. Rev. E **57**, 6962 (1998).
[5] P. Bartlett, R. H. Ottewill, and P. N. Pusey, J. Chem. Phys. **93**, 1299 (1990).
[6] P. Bartlett, R. H. Ottewill, and P. N. Pusey, Phys. Rev. Lett. **68**, 3801 (1992).
[7] M. D. Eldridge, P. A. Madden, and D. Frenkel, Mol. Phys. **80**, 987 (1993).
[8] M. D. Eldridge, P. A. Madden, and D. Frenkel, Mol. Phys. **79**, 105 (1993).
[9] M. D. Eldridge, P. A. Madden, and D. Frenkel, Nature (London) **365**, 35 (1993).
[10] J. Zhang, R. Blaak, E. Trizac, J. A. Cuesta, and D. Frenkel, J. Chem. Phys. **110**, 5318 (1999).
[11] B. Coluzzi, M. Mézard, G. Parisi, and P. Verrocchio, J. Chem. Phys. **111**, 9039 (1999).
[12] M. Mézard and G. Parisi, J. Chem. Phys. **111**, 1076 (1999).
[13] R. D. Mountain and A. C. Brown, J. Chem. Phys. **80**, 2730 (1984).
[14] J. S. van Duijneveldt and D. Frenkel, J. Chem. Phys. **96**, 4655 (1992).
[15] P. R. ten Wolde, M. J. Ruiz-Montero, and D. Frenkel, J. Chem. Phys. **104**, 9932 (1996).
[16] G. Gonnella, E. Orlandini, and J. M. Yeomans, Phys. Rev. Lett. **78**, 1695 (1997).
[17] R. D. Groot and T. J. Madden, J. Chem. Phys. **108**, 8713 (1998).
[18] R. D. Groot, T. J. Madden, and D. J. Tildesley, J. Chem. Phys. **110**, 9739 (1999).
[19] P. J. Hoogerbrugge and J. M. V. A. Koelman, Europhys. Lett. **19**, 155 (1992).
[20] J. M. V. A. Koelman and P. J. Hoogerbrugge, Europhys. Lett. **21**, 363 (1993).
[21] P. Español and P. Warren, Europhys. Lett. **30**, 191 (1995).
[22] P. Español, Phys. Rev. E **52**, 1734 (1995).
[23] M. P. Allen and D. J. Tildesley, *Computer Simulation of Liquids* (Oxford University Press, Oxford, 1987).
[24] J.-P. Hansen and I. R. McDonald, *Theory of Simple Liquids*, 2nd ed. (Academic, San Diego, 1986).
[25] J. N. Cape and L. V. Woodcock, Mol. Phys. **72**, 976 (1980).
[26] D. M. Heyes and J. G. Powles, Mol. Phys. **95**, 259 (1998).
[27] J. A. Barker and D. Henderson, J. Chem. Phys. **47**, 4714 (1967).
[28] H. C. Andersen, J. D. Weeks, and D. Chandler, Phys. Rev. A **4**, 1597 (1971).
[29] T. Boublík and I. Nezbeda, Collect. Czech. Chem. Commun. **51**, 2301 (1986).
[30] L. V. Yelash, T. Kraska, E. A. Müller, and N. Carnahan, Phys. Chem. Chem. Phys. **1**, 4919 (1999).
[31] N. F. Carnahan, E. A. Müller, and J. Pikunic, Phys. Chem. Chem. Phys. **18**, 4259 (1999).
[32] C. G. Gray and K. E. Gubbins, *Theory of Molecular Fluids* (Oxford University Press, Oxford, 1984), Vol. 1.
[33] K. E. Evans and M. D. Ferrar, J. Phys. D **22**, 354 (1989).
[34] R. M. Stratt, S. L. Holmgren, and D. Chandler, Mol. Phys. **42**, 1233 (1981).
[35] W. J. McNeil and W. G. Madden, J. Chem. Phys. **76**, 6221 (1982).
[36] R. D. Groot and P. B. Warren, J. Chem. Phys. **107**, 4423 (1997).
[37] S. Jury *et al.*, Phys. Chem. Chem. Phys. **1**, 2051 (1999).
[38] R. C. Ball and J. R. Melrose, Physica A **247**, 444 (1997).
[39] W. G. Hoover, Phys. Rev. A **31**, 1695 (1985).
[40] S. Melchionna, G. Ciccotti, and B. L. Holian, Mol. Phys. **78**, 533 (1993).
[41] T. R. Forester and W. Smith, DL_POLY molecular dynamics code, CCP5 of the EPSRC, 1995.
[42] D. Fincham, Mol. Simul. **8**, 165 (1992).
[43] L. Verlet, Phys. Rev. **159**, 98 (1967).
[44] R. W. Hockney, Methods Comput. Phys. **9**, 136 (1970).
[45] N. F. Carnahan and K. E. Starling, J. Chem. Phys. **51**, 635 (1969).
[46] J. J. Erpenbeck and W. W. Wood, J. Stat. Phys. **35**, 321 (1984).
[47] A. Malijevský and J. Veverka, Phys. Chem. Chem. Phys. **18**, 4267 (1999).
[48] T. Boublík, J. Chem. Phys. **53**, 471 (1970).
[49] G. A. Mansoori, N. F. Carnahan, K. E. Starling, and T. W. Leland Jr., J. Chem. Phys. **54**, 1523 (1971).
[50] J. A. C. Veerman and D. Frenkel, Phys. Rev. A **45**, 5632 (1992).
[51] M. Dijkstra, D. Frenkel, and J.-P. Hansen, J. Chem. Phys. **101**, 3179 (1994).
[52] P. J. Camp, M. P. Allen, P. G. Bolhuis, and D. Frenkel, J. Chem. Phys. **106**, 9270 (1997).
[53] D. Frenkel, J. Phys.: Condens. Matter **6**, A71 (1994).
[54] S. D. Group, GEOMVIEW, Geometry Center, 1300 South 2nd Street, Suite 500, Minneapolis, MN 55454.
[55] S. Nosé, Mol. Phys. **57**, 187 (1986).